Real-time shallow landslide hazard assessment on a regional scale

Xiaohui Qi[1], Joao Mendes[1], Rupert Bainbridge[2], Stuart Dunning[2], Mike G. Winter[3], and Michael Lim[1]

[1]Department of Mechanical and Construction Engineering, Northumbria University, Newcastle Upon Tyne, NE1 8ST, UK

[2]Department of Geography, Newcastle University, Newcastle, NE1 7RU, UK.

[3]Winter Associates, Kirknewton, Midlothian, EH27 8AF, UK.

Email: xiaohui.qi@northumbria.ac.uk (X Qi), joao.mendes@northumbria.ac.uk (J Mendes), rupert.bainbridge@newcastle.ac.uk (R. Bainbridge), stuart.dunning@newcastle.ac.uk (S. Dunning), mwinter@winterassociates.co.uk (M Winter), michael.lim@northumbria.ac.uk (M Lim)

Abstract: Shallow landslides are a major natural hazard in the UK, causing more than £10M of economic losses annually and posing clear threats to life. Rainfall is an essential control on shallow landslide risk, but network operators currently use generic 'on-off' warnings based on localised rainfall intensity and duration, giving no strategic information about where the hazard is highest or evolving the quickest for any particular rainfall event. A new procedure has been developed to automatically evaluate the stability of slopes across regional scales in response to spatially and temporally variable rainfall events, quantified by rainfall radar data updated every 5 minutes. A physically based programme, TRIGRS, was used to assess the factor of safety (FS) of slopes in response to spatially variable rainfall radar data. The dynamic FS maps produced provide early warning and informed decision-making for the management of regional to national-scale infrastructures. Sensitivity analyses were performed to investigate the effect of the soil thickness, shear strength parameters, hydraulic parameters, and antecedent rainfall on the FS during a known landslide-causing rainfall event in Glen Croe, western Scotland. The results specifically highlight the slope where the failure occurred as a high-hazard area 1.0 hour

before the event. The dynamic FS maps were particularly sensitive to soil thickness, the saturated hydraulic diffusivity and Gardner's unsaturated conductivity, suggesting that more effort should be put into improving network-scale datasets of these parameters. Ultimately, the ability developed here to account for near-real-time spatial variabilities in rainfall data and slope responses measured through the relative change in FS values provides a potentially transformative new tool for network operators to proactively mitigate the impacts of specific storms as they develop.

Keywords: Real-time hazard assessment; dynamic hazard maps; early warning systems; shallow landslides; rainfall radar data

Introduction

On average, about 28 landslides are reported every year in the UK and the financial losses incurred are estimated to exceed £10 million per year, a figure that is expected to grow in the future due to climate change (Gibson et al. 2013). The economic impacts of landslides that affect transport networks can include severance of access to and from relatively remote communities for services and markets for goods; employment, health and educational opportunities; and social activities (Winter et al. 2019b) and those impacts can extend over very significant areas (Klose et al. 2015; Winter et al. 2019b). Physical damage to vulnerable infrastructure (Winter et al. 2014; Argyroudis 2019) can be associated with significant repair times thus magnifying the economic impacts.

Lee and Giles (2020) note that the occurrence of landslides in the UK is typically linked with rainfall and this effect is amplified when shallow landslides such as debris flows (Winter 2020) are considered. However, direct triggers are often not possible to determine as rainfall events of similar magnitudes and intensities produce different outcomes (Winter et al. 2010, 2019a; Bainbridge et al. 2022). This uncertainty makes it extremely difficult for road and rail network operators, and other regional-scale infrastructure owners and operators, to make informed decisions on where or when risks of failure might be particularly high. Consequently, much of the management of landslide hazards is responsive and reactive to failure events. Quantitative risk assessment can articulate the risk of fatalities on a timescale that relates to the processes in play and is independent of the usually rather limited timespan over which human knowledge is robust (e.g., Winter and Wong 2020). Accordingly, there is a need for improved information on the spatial distribution of landslide susceptibility across wide areas and to correlate that information in near real-time, with specific rainfall events to identify the highest hazard locations to help target close monitoring, preventative or mitigative efforts.

Regional landslide assessments aim, at least initially, to assess the susceptibility of the slopes to failure or to identify the rainfall threshold of the landslides within a region (Segoni et al. 2018). The approaches used can be divided into two categories: empirically based methods and physically based methods. Empirically based methods (such as statistical or regression methods) employ empirical equations to express the relationships between landslide susceptibility and causal factors such as hydrogeological conditions and landslide responses (e.g., Ayalew et al. 2004; Remondo et al. 2005; Liu and Wu 2008, Harrison et al. 2008; Mathew et al. 2009; Baeza et al. 2010; Erener and Düzgün 2010; Akgun 2012; Felicísimo et al. 2013). For example, network operators currently rely on generic 'on-off' warnings based on rainfall intensity and duration for specific slopes within a local area. The main disadvantage of empirically based methods is that they disregard spatially and temporally distinct physical processes causing landslides such as the hydraulic response of different soil types to rainfall. As a result, the dynamic nature of the landslide hazard under a specific rain event cannot be captured. The empirically based methods give no strategic information about where the hazard is highest or evolving the quickest for any particular rain event. Physically based methods include the use of limit equilibrium or finite element methods to evaluate slope stability as well as the hydraulic response of the slope to rainfall (e.g., Borga 1998; Teixeira et al. 2005; Arnone et al. 2011; Chen and Zhang 2014; Teixeira et al. 2015; Hsu et al. 2018; Marin 2020). These numerical methods were used to derive the rainfall intensity and duration thresholds, perform early warning of landslide hazards using the factor of safety (FS) index, or evaluate the probability of failure of slopes. They provide a physically meaningful susceptibility assessment of slope stability but can be data-intensive and computationally expensive where large data volumes such as topographic, geotechnical, and geological information are required; they are thus less well-suited to regional assessments.

There remain critical drawbacks limiting effective susceptibility or hazard assessments of landslides. Firstly, the relative likelihood of slope failure changes dynamically through time and across space during a rainfall event, due to the uneven distribution of water across the region. Real-time slope hazard assessments methods incorporating temporally varying rainfall intensity have been proposed for localised areas (e.g., Xie et al. 2004; Bainbridge et al. 2022), limited by data availability and transferability to wider regional scales. Advances have been made using real-time rain gauge data to assess landslide hazard (e.g., Montrasio et al. 2011; Chen and Zhang 2014; Canli and Glade 2016; Chen et al. 2016; Zieher et al. 2017; Dikshit et al. 2019), but rain gauge networks typically achieve sparse coverage and comparability, and extrapolation can be challenging. Kirschbaum and Stanley (2018) combined satellite-based precipitation estimations with a landslide susceptibility map to identify the landslide hazard in near real-time, but the precipitation data have a low pixel resolution (i.e., 0.1° ≈ 11 km) and frequency (i.e., 30 min) and the accuracy of landslide detections thus is low. In addition, the susceptibility of different slopes within an area of interest (at any scale) is controlled by site-specific factors that determine how the water is distributed and then propagates. For example, the same rainfall event is likely to induce variations in the surface runoff on slopes of different gradients, altering the hydraulic response within the soil and thus associated susceptibility. Therefore, a single, static rainfall threshold is likely to become increasingly less effective for the wider or more complex area of concern. It is worth noting that probabilistic slope stability analysis could be one potential solution to address the uncertain slope response, but it is normally computationally expensive and the estimation of the inherent variability parameters of the soil properties, such as the mean value, standard deviation, and scale of fluctuation, which are key inputs of probabilistic analyses, requires large quantities of soil data.

This paper proposes a new near-real-time hazard assessment procedure for slope stability using national databases of model parameters and rainfall radar. The outcomes demonstrate the

potential to proactively target responses to evolving landslide hazards by accounting for the actual distribution of live (or forecast or simulated) rainfall events, potentially at any scale. In particular, this study highlights the change in the FS (δ_{FS}) as well as the actual FS value as being the critical metrics of landslide hazards as δ_{FS} is less sensitive to the initial parametric values than FS. This paper is organized as follows. Firstly, the proposed procedure for near-real-time regional-scale hazard shallow landslide assessments is illustrated. Secondly, the procedure was applied to a known rainfall-triggered landslide case and its effectiveness is evaluated by comparing the dynamic FS maps with the actual landslide locations and timing. The sensitivity of the FS maps to various factors is investigated to account for the uncertainty of the input physical parameters.

Developing near-real-time regional-scale hazard assessment for shallow landslide

This section presents the proposed procedure for a near-real-time regional-scale shallow landslide hazard assessment. The procedure uses a physically based program, TRIGRS (Baum et al. 2002) to assess the slope stability and rainfall radar data to account for the spatio-temporal variability of rainfall intensity. The proposed stages are detailed below, and the procedure is summarized in Fig. 1.

Stage 1: cell partition. The area to be investigated is divided into cells, with the cell size determining the resolution of the hazard map. The selection of the cell size is a trade-off between the map resolution and computational time as a small cell size leads to a high resolution of the map but significantly increases the computational time.

Stage 2: data preparation. The required data for network-scale slope stability analysis includes geotechnical, geological, topographical and meteorological data. The geological data mainly refer to the superficial deposit thickness to be used in slope stability analysis. The topographical data were downloaded from the digital terrain model of the Ordnance Survey (https://www.ordnancesurvey.co.uk/business-government/products/terrain-5) while soil type

and superficial deposit thickness data were from Edina Digimap (https://digimap.edina.ac.uk/). These data sets have full national coverage of Great Britain. The topographical data and the thickness data have a spatial resolution of 50 m. The superficial deposit thickness database was derived from the British Geological Survey (BGS) archive borehole records using interpolation algorithms (Lawley and Garcia-Bajo 2009). Where necessary, spatial interpolation is used to extrapolate the most likely values at the centres of the cells created in Stage 1. The slope angle and aspect are derived using the "Spatial Analyst tool" in the ArcMap (ArcGIS Desktop 10.5, ESRI 2016) and used to specify the connectivity between a cell and adjacent downslope cells.

Rainfall data for each cell are taken from the Met Office's UK rainfall radars via the Met Office NIMROD system, a very short-range forecasting system providing forecasts of up to six hours (https://catalogue.ceda.ac.uk/uuid/27dd6ffba67f667a18c62de5c3456350). The system processes radar and satellite data, together with surface reports and numerical weather prediction fields to obtain the precipitation rate at a resolution of 1 km and a frequency of 5 minutes.

It is impractical to achieve sufficient spatial coverage of such data to provide for network-scale analyses. Therefore, geotechnical parameters are assumed based on the soil types and parametric values reported in the literature (e.g., Milne 2008; Cascini et al. 2015; Gioia et al. 2016; Clarke BG 2018; Hsu and Liu 2019). TRIGRS uses four parameters to approximate soil-water characteristic curves for unsaturated soils in the focus area and to derive the dynamic hydraulic conductivity $K(\cdot)$, as given by:

$$\theta = \theta_r + (\theta_s - \theta_r)\exp(\alpha\psi^*) \tag{1a}$$

$$K(\psi) = K_s \exp(\alpha\psi^*) \tag{1b}$$

where θ, θ_r, and θ_s denotes the volumetric water content, residual volumetric and saturated volumetric water content, respectively; $\psi^* = \psi + 1/\alpha$, in which ψ is the pressure head; α is a constant which can be obtained by fitting Eq. 1b to data points of (pressure head, volumetric

water content); K_s is the saturated hydraulic conductivity. Eq. 1b is called Gardner's (1958) unsaturated conductivity model. The value of α can also be derived from other commonly used soil-water characteristic models such as the van Genuchten (VG) model, as shown in Marin (2020) and Marin et al. (2021). Along with the four hydraulic parameters, other soil properties data include shear strength parameters (i.e., friction angle and cohesion), unit weight, and diffusivity (e.g., Milne 2008; Cascini et al. 2015; Gioia et al. 2016; Clarke BG 2018; Hsu and Liu 2019).

Stage 3: calculation in TRIGRS. The TRIGRS uses an analytical solution for partial differential equations to compute the transient pore-pressure changes and a simple infinite-slope model to compute the factor of safety on a cell-by-cell basis. The outputs include time-varying FS, time-varying suction, failure time, and critical slip depth. Further details for the methods for seepage and slope analyses in TRIGRS can be found in Baum et al. (2002). There are inevitably varied levels of uncertainty associated with the input parameters, such as the initial condition of pore water pressure, initial water table and the thickness of soils overlying the rock layer. Therefore, here this study emphasises the change in the FS as well as the actual FS value as being the critical metrics.

Stage 4: dynamic FS map production. The dynamic maps of FS on slopes across the area of interest are analysed to target particular areas of concern across the network during current or forecast rainfall events and to initiate strategic decisions or early warnings for the areas with high hazards to that particular distribution and sequence of rainfall.

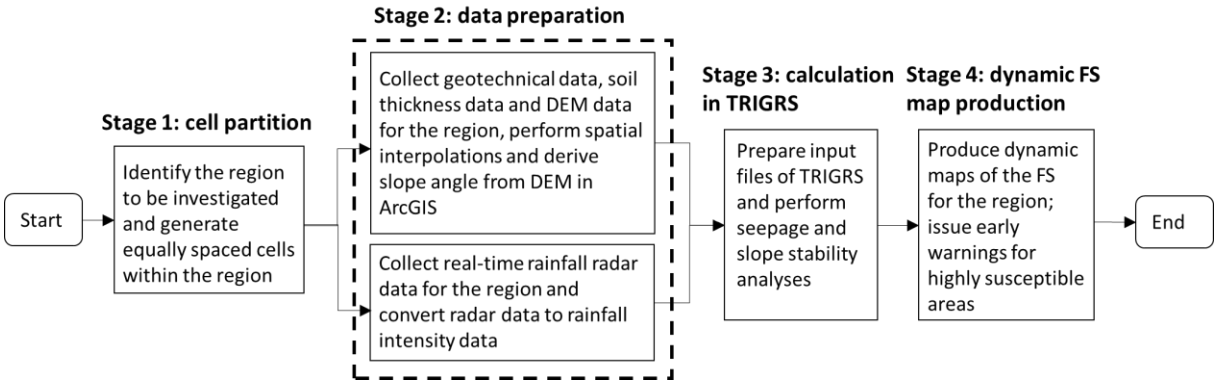

Fig. 1. Flowchart of the new procedure for near-real-time hazard assessments for shallow landslides across wide areas.

Application to real landslide hazards

The new procedure has been applied to the A83 Rest and Be Thankful (RabT), a problematic landslide hazard site within the Glen Croe in western Scotland. Fig. 2 presents the investigated watershed as well as the superficial deposit thickness of the area. The geological, geometrical, geotechnical and rainfall data information available has been extracted from datasets with national coverage, making the approach transferrable to other UK sites. The watershed has been divided into 16256 cells of 200 m × 200 m. This cell size is a trade-off between the accuracy of the FS map and the computational efficiency. A smaller cell size leads to a more precise identification of the high-hazard area, but the overall distribution of the landslide hazard does not change significantly. If more precise hazard information is required, it would be more efficient to firstly use coarser-resolution analyses to identify vulnerable (e.g., areas with FS < 2) areas and then perform higher-resolution (such as 50 m) slope stability analyses at the vulnerable areas. As shown in Fig. 2, the A83 is a major arterial road surrounded by steep slopes (the steepest slope has a slope angle as high as 42.2°).

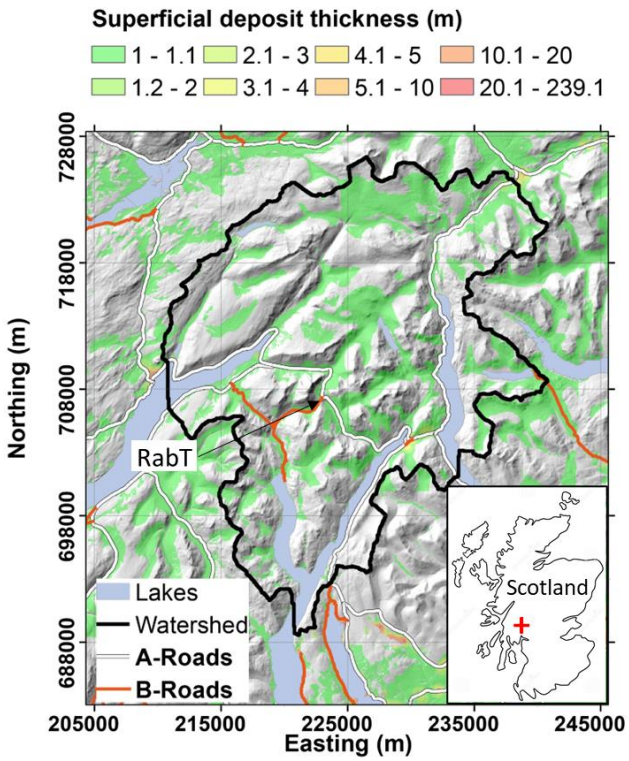

Fig. 2 Superficial deposit thickness of the investigated watershed in Western Scotland, UK, derived from the British Geological Survey and obtained from the online database Digimap (digimap.edina.ac.uk), overlain on a topographic hillshade map of the region (UK national grid coordinate system).

Several types of superficial deposits, such as till, alluvium, peat and river terrace deposits, can be found in the watershed. However, since most of these deposits are constituted of coarse-grained soils such as sand and gravel, the geotechnical parameters for the superficial deposits were assumed to be similar and are summarized in Table 1. These values were assumed according to parametric values reported in the literature (e.g., Milne 2008; Cascini et al. 2015; Gioia et al. 2016; Clarke BG 2018; Hsu and Liu 2019).

Table 1 Geotechnical parameters

Parameter	Values
Cohesion, c (kPa)	6
Friction angle, ϕ (^{o})	30
Saturated hydraulic conductivity, *Ks* (m/s)	8×10^{-6}
Saturated hydraulic diffusivity, D_0 (m^2/s)	8×10^{-5}
Gardner's unsaturated conductivity model parameter, α (m^{-1})	1
Saturated volumetric water content, θ_{sat}	0.45
Residual volumetric water content, θ_{res}	0.05
Unit weight of soil (kN/m^3)	22

Most of the soil deposits in the watershed have a thickness of around 1 m, a value that was used in the analysis for all soil deposits. It should be noted that certain areas within the watershed have soil deposits as thick as 10 m and could be more susceptible to deep slope failures than shallow failures that provide the focus for this work. The unshaded areas, i.e., the areas without superficial deposits, in Fig. 2, were considered to be bedrock. The major rock formation found in the watershed area is the Neoproterozoic schistose psammites and semipelites belonging to the Beinn Bheula Schist Formation of the Southern Highland Group (BGS, 1987).

In recent years, landslide events have led to the repeated closure of the A83 RabT Road that passes through the valley midway up the slope (Bainbridge et al. 2022) and there is an old military road near the slope base that is used as a single carriageway alternative when landslides, or the threat of landslides impact the main road. Fig. 3 shows the location of landslides that have occurred at the site during the year 2015~2020. These locations were identified by analysing satellite images on different dates using Google earth engine (e.g., Handwerger et al. 2020; Prasetya et al. 2021). This study focuses on a particularly well time-constrained landslide (Landslide A) that occurred on October 31, 2020, at 10:00 am, as highlighted in Fig. 3.

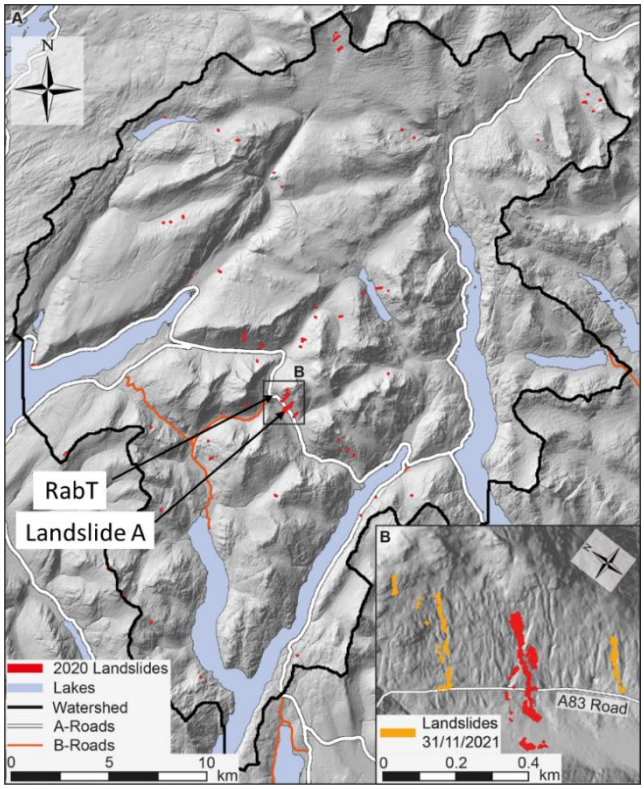

Fig. 3 Location of landslides detected by satellite

Accounting for the spatial distribution of rainfall

Two types of rainfall data for the watershed area have been analysed, namely data from a rain gauge located at the site and data derived from rainfall radar. The precipitation rate at a resolution of 1 km and a frequency of 5 minutes has been obtained from the Met Office NIMROD system and compared to 15-minute-frequency rainfall data from a rain gauge located approximately 1 km west of the landslide area. The rain gauge data were collected by Scottish Environment Protection Agency's automated rain gauge at the site.

Fig. 4(a) presents the rain gauge data and the storm rainfall radar data at the cell corresponding to the landslide location and rain gauge location, starting one day before the event until its occurrence (October 31st, 2020). For validation, the frequency of the rainfall radar data is transformed from 5 min to that of the rain gauge data, i.e., 15 min by averaging rainfall intensities at three successive time points. As shown, the rain gauge data are generally consistent with the site-specific radar data, in both the rainfall-intensity-peak occurrence time

and in peak magnitudes, for both days. The rainfall intensity for Oct 30, 2020, is much lower than that for the following day, the day the landslide occurred. Before the storm event associated with the landslide relatively little rain was recorded but the storm comprised a sustained period of heavy rainfall with an initial peak at hour -6 and larger peaks at hours -2 and -1.

Fig. 4(b) presents the spatial distribution of rainfall data, which progresses from being largely concentrated in the east and upper peaks of the catchment at hours -7 and -4 to being highly concentrated at the landslide location at hours -1 to +1 when peak rainfall intensity occurred (identified in Fig. 4(a) by the vertical grey dashed lines). Such variability of the rainfall intensity is caused by the prevailing storm direction moving from the southwest towards the northeast of the catchment.

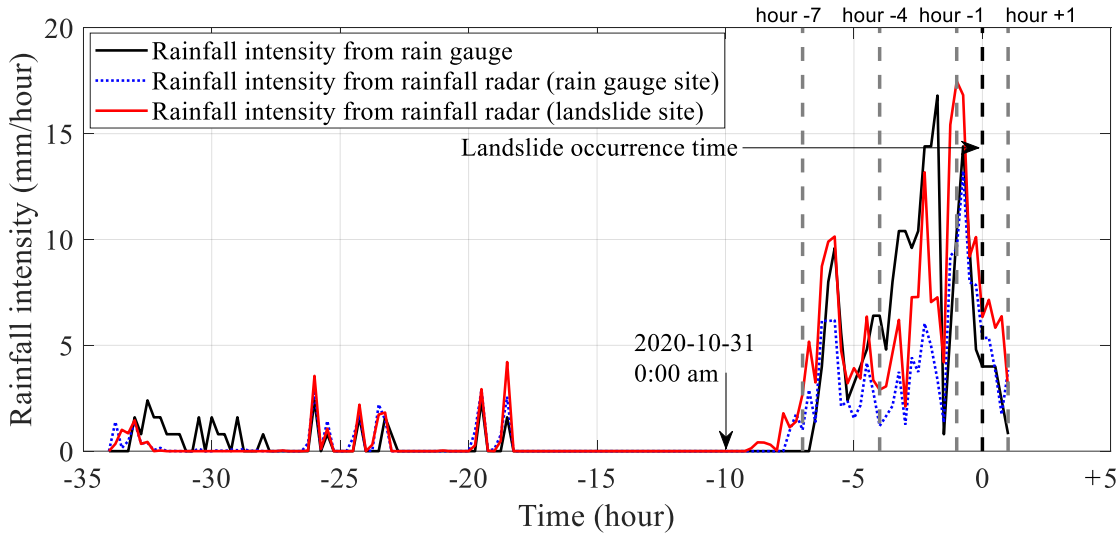

(a) Rainfall intensity varying with time

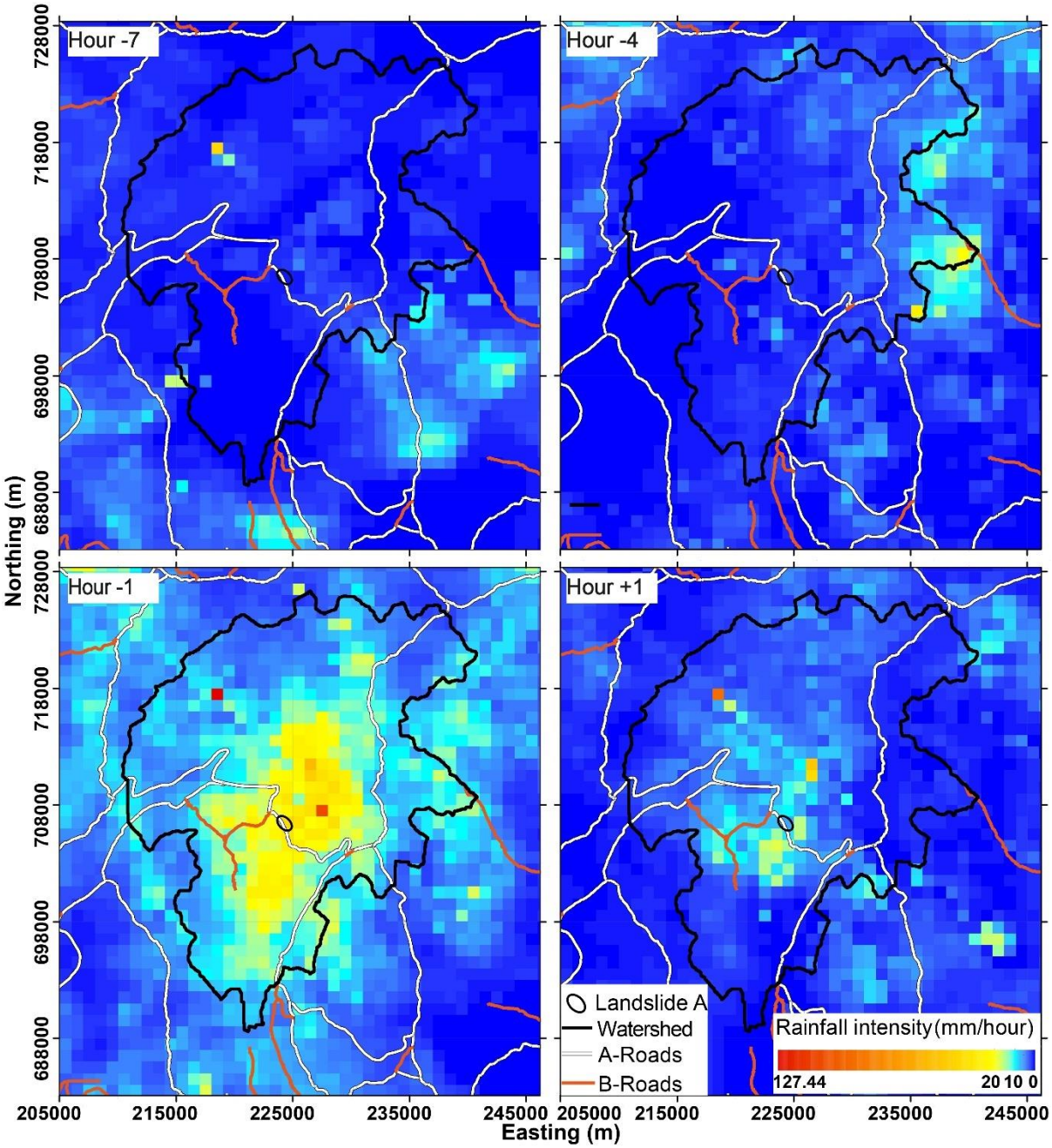

(b) Rainfall radar data

Fig. 4 Rainfall intensity at different times during the landslide-inducing storm

The initial water table was considered to be located at the bottom of the soil layer and the lower boundary of the soil layer was taken to be impermeable underlying rock. The initial condition was obtained by performing a steady seepage analysis based on the assumed depth of the initial water table. The soil thickness of the superficial deposit was taken to be 1 m (see

Fig. 2; Bainbridge et al. 2022) unless the area was classified as rock with very limited soil, where a soil thickness of 0.1 m was assumed to account for a thin, weathered layer.

An initial comparison was run between the spatially constant rainfall intensity data (Case 0b) from the rain gauge and the spatially variable radar data (Standard Case: case 0a) with the same initial conditions assumed (Table 2).

Table 2 Cases for illustrating the proposed procedure

Cases	Soil thickness (m)	c (kPa)	ϕ (°)	Ks (m/s)	α (m^{-1})	D_0 (m^2/s)	Depth of initial water table (m)	Rainfall	Antecedent rainfall
Standard Case: Case 0a	1 m for superficial deposit and 0.1 m for rock layer	6	30	8×10^{-6}	1	8×10^{-5}	1	Spatially varying rainfall radar data	0
Case 0b	1 m for superficial deposit and 0.1 m for rock layer	6	30	8×10^{-6}	1	8×10^{-5}	1	Spatially constant rainfall intensity (rain gauge)	0

The FS maps at hours -7, -4, -1 and +1 (immediately after the Landslide A event) for Standard Case 0a are shown in Fig. 5. The FS maps are overlain on the map representing the superficial deposits present at the site. Accounting for the uncertainties in the initial parameters at this particular site, the critical FS value was considered to be 1.2 (represented by the red colour). As shown by the increased number and size of red areas in the FS maps as time elapses, the FS in the watershed generally reduces with time. The high-hazard areas (defined as areas with FS <1.2) at one hour before failure are highly consistent with the landslide sites shown in Fig. 3, including the known event (Landslide A) and several smaller landslides that occurred during this particular storm. More importantly, the FS maps highlight the potentially problematic slopes for network operators to focus attention on, which account for a small percentage (< 1%) of slopes in the watershed. This facilitates better planning and more targeted allocation of the resources and implementation of early warning measures of landslide hazards. Note that one high-hazard slope is detected by the FS map at the location of (easting, northing)

= (229700 m, 710900 m) (see site (ii) in Fig. 5), but no slope failures were observed at the same location on the landslide detection map in Fig. 3. The reason may be the inaccurate soil properties used in slope stability analyses or that very small-scale landslides cannot be detected from the satellite images.

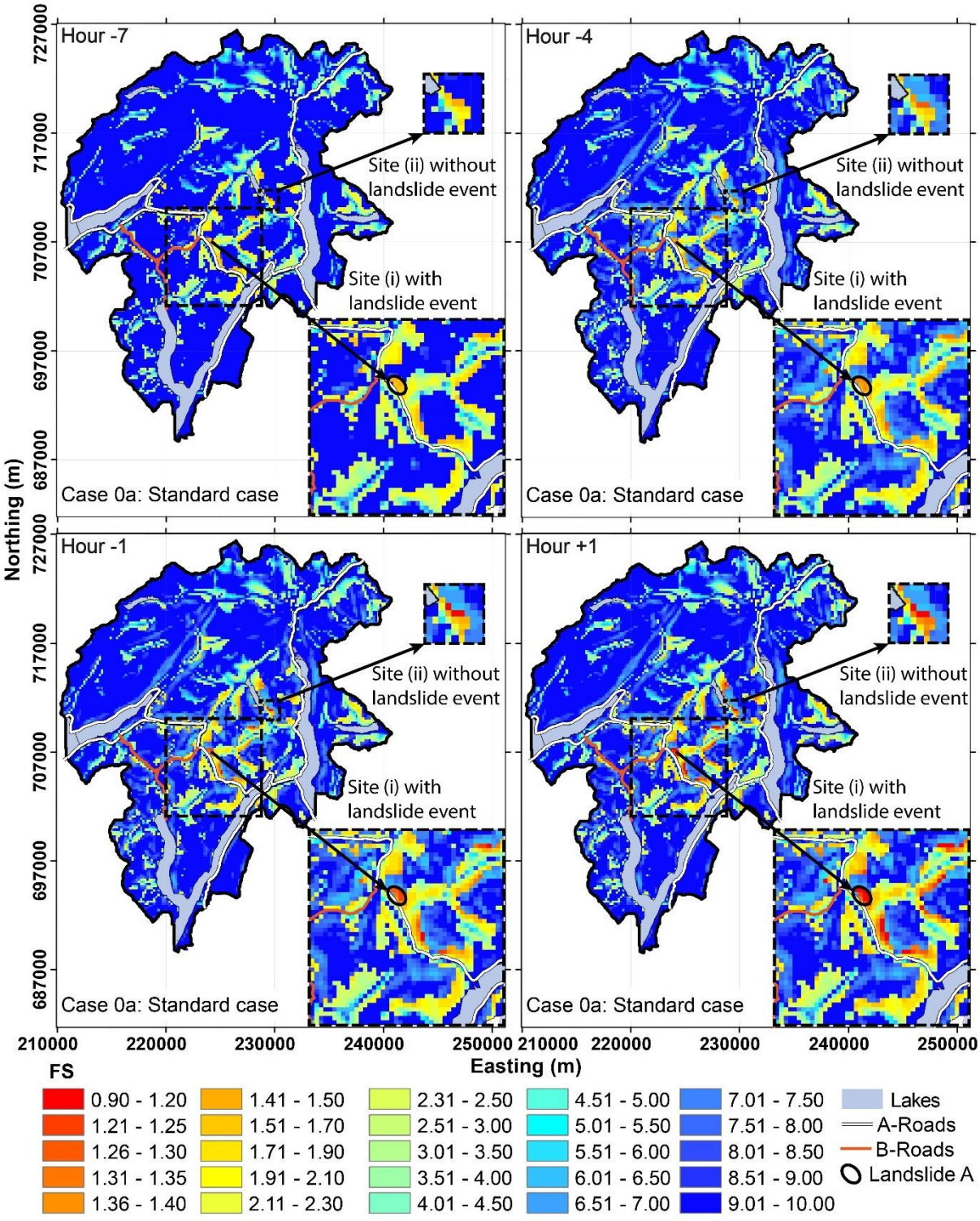

Fig. 5 Evolution of factor of safety maps across the storm event for the Standard Case, Case 0a

In reality, it is important to observe the evolution of the FS and for slopes where failure may be possible. Rapid or significant changes in FS could be more effective than set threshold values for early warning applications. Fig. 6(a) plots the frequency of the FS for slopes with an initial FS at hour -10, $FS_{-10} < 3$ and the FS variation relative to FS_{-10}, δ_{FS}= FS-FS_{-10}, for slopes with $FS_{-10} < 1.6$. These plotted slopes represent relatively high-hazard slopes in the presence of the large uncertainties in the physical parameters. Only 6 slopes have FS less than 1.2 while 20 slopes have an $FS_{-10} < 1.6$ and $\delta_{FS} < -0.2$ at hour -1. This is equivalent to 0.5% and 1.8% of all the 1140 slopes with $FS_{-10} < 3$, respectively, demonstrating the effectiveness of the proposed procedure in focussing attention on the high-hazard slopes for a specific event. Fig. 6(b) plots the variation of the percentage of high-hazard slopes with time. The high-hazard slopes represent the possibly problematic slopes with $FS < 1.2$ or $\delta_{FS} < -0.2$ with $FS_{-10} < 1.6$ while the percentage is the ratio of the number of high-hazard slopes to the number of slopes with $FS_{-10} < 3$ (i.e., 1140). The percentage of the high-hazard slopes shows the evolution of the slope hazard in the watershed but remains a low proportion of the catchment area. For instance, 28 slopes have $FS < 1.2$ at hour +1, accounting for 28/1140 = 2.5% of the slopes with $FS_{-10} < 3$ and 28/16256 = 0.17% of the catchment area. Furthermore, an early warning can be issued as shown in Fig. 7, which shows the critical areas determined based on the magnitude of FS and δ_{FS} 1 hour (hour -1) before the landslide occurrence. As shown, the area with significant changes in FS is also consistent with the Landslide A location, indicating the effectiveness of this early warning strategy based on δ_{FS}.

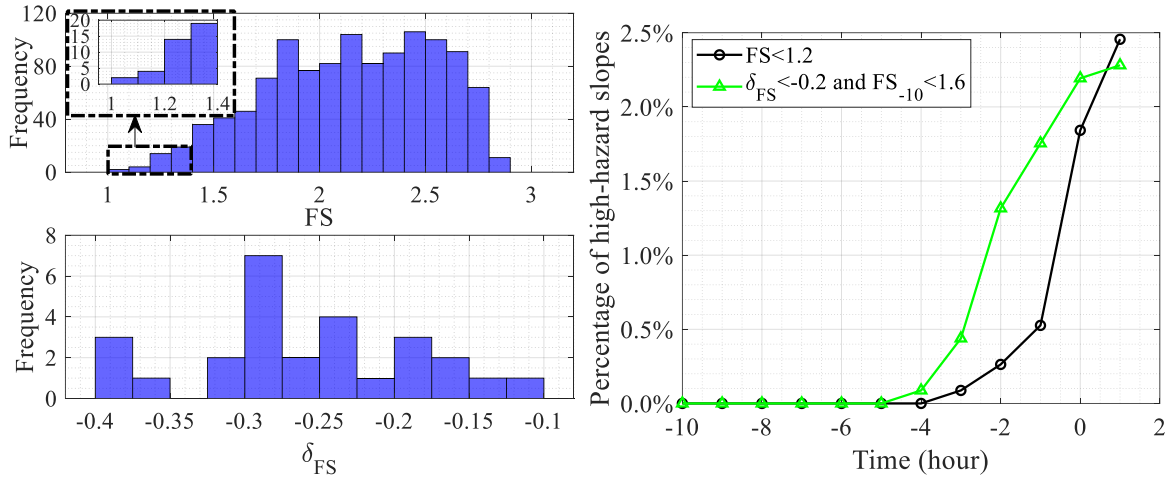

(a) FS and δ_{FS} (FS$_{-10}$ < 1.6) at hour -1 (b) Percentage of high-hazard slopes

Fig. 6 Frequency of FS and δ_{FS} for the standard case at 1 hour before Landslide A failure and evolution of the percentage of high-hazard slopes with time

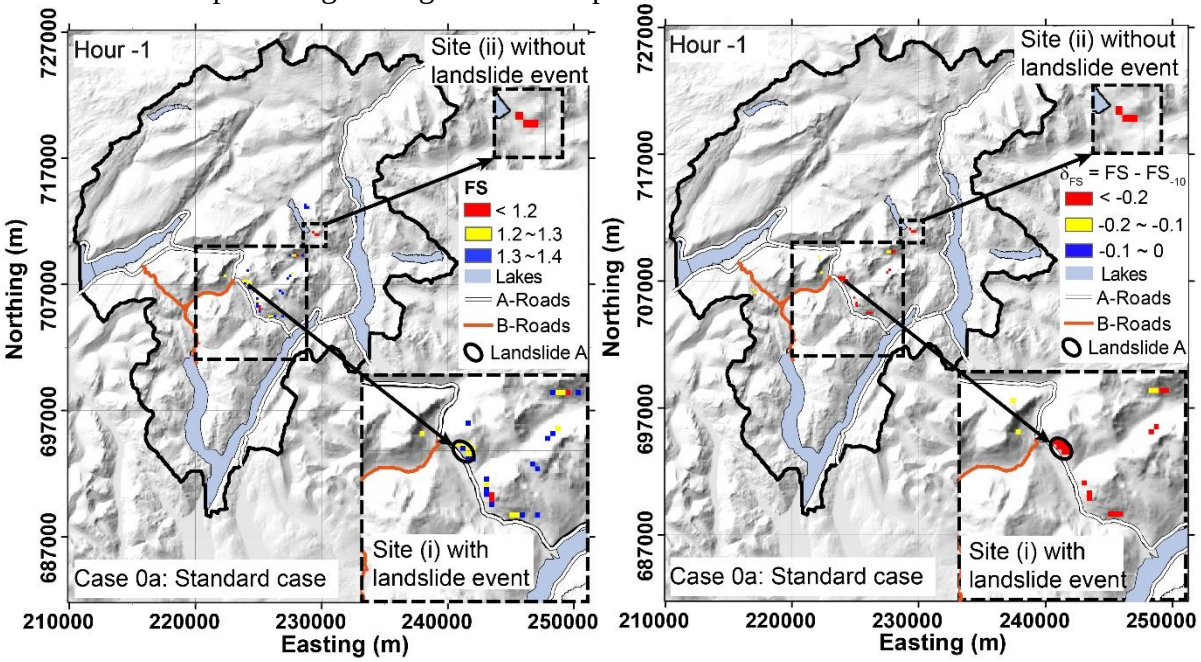

(a) Early warning using FS map (b) early warning using the map of δ_{FS}= FS-FS$_{-10}$

Fig. 7 Early warning of landslide hazards based on FS and δ_{FS} maps at 1 hour before Landslide A failure

Fig. 8(a) shows the ΔFS (FS-FS$_{standard}$, i.e. the difference of FS for any case and the Standard Case, Case 0a) map at 1 hour after Landslide A failure (hour +1) for case 0b with spatially constant rainfall (i.e., use rain gauge data) while Fig. 8(b) presents the FS variation with time for the slope at the landslide site for cases 0a and 0b. The close agreement of the FS calculated through the rainfall event using radar data with that using a local rain gauge (Fig. 8(b)) effectively validates the radar data. However, the spatial limitations of using rain gauge

data are also evident, making the FS for slopes far away from the rain gauge highly biased (ΔFS can be as large as 1.6).

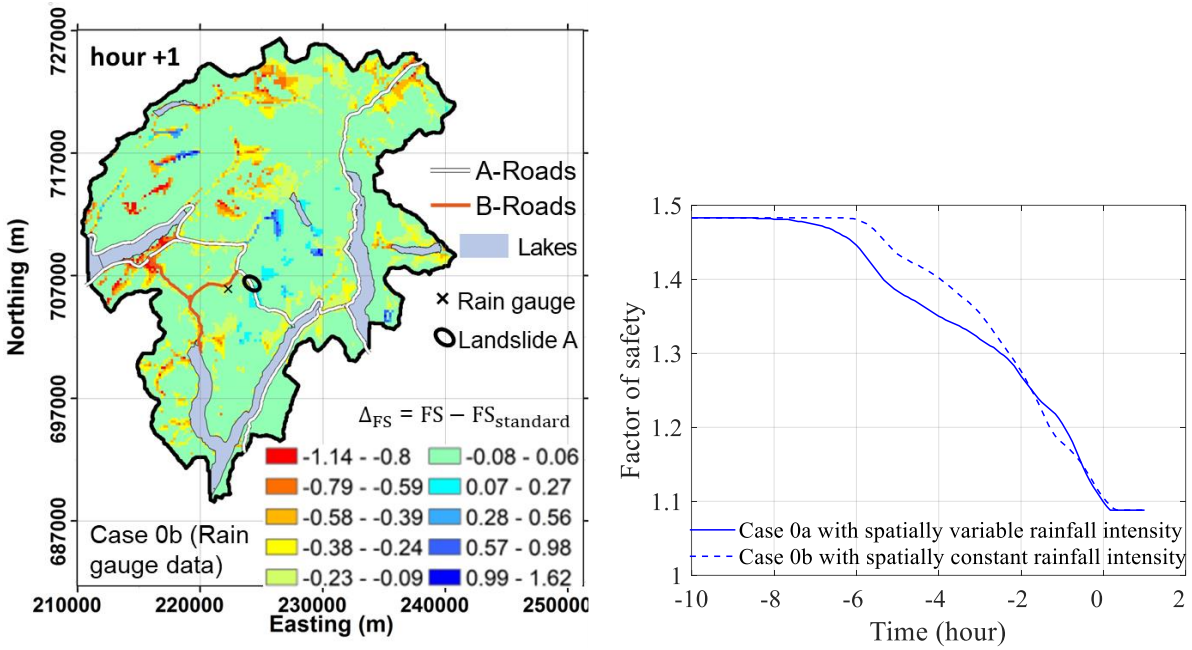

(a) ΔFS map at hour +1 (b) FS variation with time

Fig. 8 Variation of factor of safety (ΔFS) relative to the standard case for Case 0b with spatial constant rainfall intensity

Parameterisation and significance analyses

The assumed physical parametric values could potentially vary significantly from the actual values because of the limited resolution and accuracy of existing information and the natural heterogeneity of soil properties. Therefore, it is important to have an understanding of the sensitivity of the FS maps to the various input parameters, which may also focus network operator effort at improving data on the most influential parameters. This section presents four sets of cases to investigate the significance of soil thickness, shear strength parameters, hydraulic parameters, and antecedent rainfall events on the landslide hazard map produced. The four sets of cases are summarized in Table 3. Note that the effects of the saturated volumetric water content and residual water content are not presented as they were found to have a neglectable effect on the FS for this site because of the relatively shallow soil layers found throughout the area.

Set 1 contains two cases, which make different assumptions on the soil thickness overlying the rock but adopt the same soil properties and rainfall conditions as in Standard Case 0a. In Case 1a, a constant soil thickness was considered across the entire watershed. Case 1b considers the areas classified as rock layers as unweathered, exposed rock, modelled with a lower Ks value and a shear strength value higher than the soil deposits.

Set 2 contains two cases with varying shear strength parameters but the same thickness for the soil deposits, hydraulic parameters and rainfall intensity as the Standard Case. The superficial deposits mostly consist of coarse-grained soils so relatively low values of cohesion and high values of friction angles have been selected.

Set 3 contains four cases with different hydraulic parameters (Ks, α, D_0 and initial water table depth), but the other parameters remained the same values as the Standard Case. For Case 3a, the value of Ks was reduced to 2×10^{-6} m/s, which is a reasonable value for coarse-grained soil. For Case 3b, a value of 5 m^{-1} has been used for α, which ranges from 1 to 10 m^{-1} (Gioia et al. 2016). For Case 3c, the value of D_0 was set to 50Ks, which is within the normal range of D_0, i.e., from 10 Ks to 100 Ks (Ku et al. 2017). For Case 3d, a shallower initial water table than that of the Standard Case (i.e., initial water table depth = 0.5 m) was considered.

Table 3 Different cases for sensitivity analyses

Case set	Cases	Soil thickness (m)	c (kPa)	ϕ (°)	Ks (m/s)	α (m^{-1})	D_0 (m^2/s)	Depth of initial water table (m)	Rainfall	Antecedent rainfall (m/s)
Set 1: Thickness set	Case 1a (Uniform soil thickness)	1 m across the region	6	30	8×10^{-6}	1	8×10^{-5}	1	Spatially varying	0
	Case 1b (Bare rock)	1 m for superficial deposit and 0 m for rock layer	6	30	8×10^{-6}	1	8×10^{-5}	1	Spatially varying	0
Set 2: Shear strength set	Case 2a (Reduced cohesion)	1 m for superficial deposit and 0.1 m for rock layer	4	30	8×10^{-6}	1	8×10^{-5}	1	Spatially varying	0
	Case 2b (Reduced frictional angle)	1 m for superficial deposit and 0.1 m for rock layer	6	25	8×10^{-6}	1	8×10^{-5}	1	Spatially varying	0
Set 3: Hydraulic parameter set	Case 3a (Reduced Ks)	1 m for superficial deposit and 0.1 m for rock layer	6	30	2×10^{-6}	1	8×10^{-5}	1	Spatially varying	0
	Case 3b (Increased α)	1 m for superficial deposit and 0.1 m for rock layer	6	30	8×10^{-6}	5	8×10^{-5}	1	Spatially varying	0
	Case 3c (Increased D_0)	1 m for superficial deposit and 0.1 m for rock layer	6	30	8×10^{-6}	5	4×10^{-4}	1	Spatially varying	0
	Case 3d (Shallower initial water table)	1 m for superficial deposit and 0.1 m for rock layer	6	30	8×10^{-6}	5	8×10^{-5}	0.5	Spatially varying	0
Set 4: Antecedent rainfall set	Case 4 (Antecedent rainfall)	1 m for superficial deposit and 0.1 m for rock layer	6	30	8×10^{-6}	1	8×10^{-5}	1	Spatially varying	2 hours, intensity = 4×10^{-6}

Set 4 contains one case with a different scenario for rainfall precedence while maintaining the remaining parameters as the Standard Case. The antecedent rainfall has a duration of 2 hours and an intensity of 4×10^{-6} m/s. The antecedent rainfall was artificially imposed due to the lack of significant real rainfall events during the 24 hrs preceding the day of landslide occurrence (i.e., 30th October 2020; Fig. 4(a)).

Effect of soil thickness

It should be noted that the underpinning principle of the model is that of an infinite slope where the length is large compared to the depth of the soil, making it particularly applicable to shallow failures. The shallow slopes are focused on herein as it is shallow slope failures that cause most of the disruption in the UK. The soil thickness data are relatively uniform across the study area and so have been modelled accordingly, but the model can include spatially variable soil thickness if appropriate at other sites. The map of FS for Case 1a with a uniform soil thickness at 1 hour after the landslide failure is shown in Fig. 9. In contrast with the Standard Case (Fig. 5), the high-hazard areas (FS <1.2) became more pronounced when uniform soil thickness was applied over the whole region. The simplification to a single soil layer thickness generally relatively underestimates the FS and produces unrealistically high coverage of high-hazard areas.

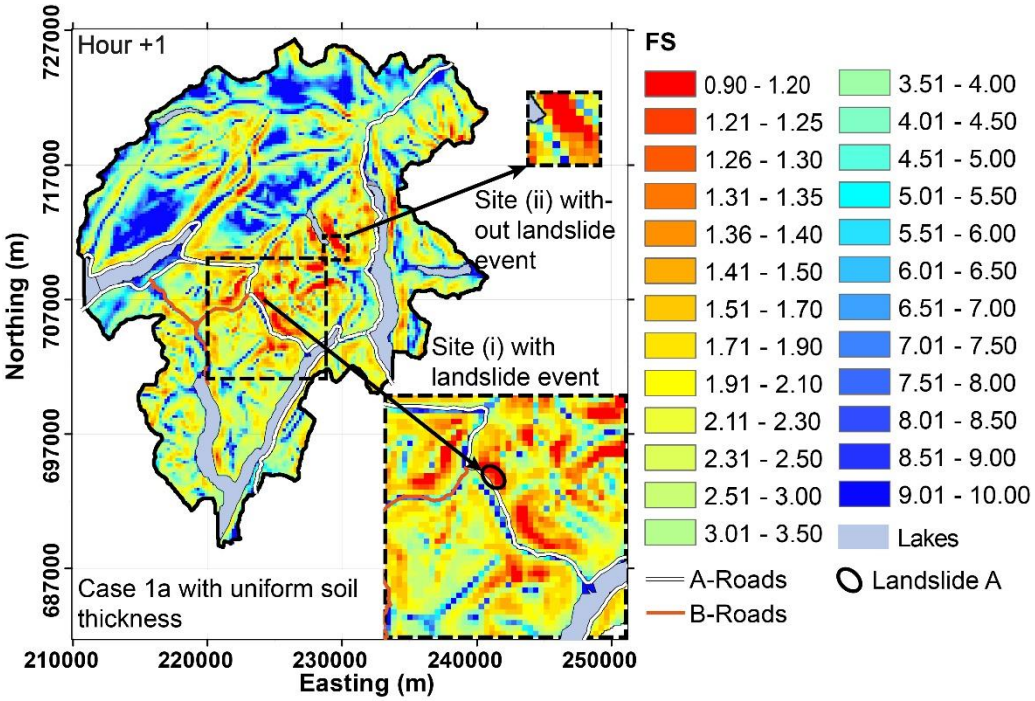

Fig. 9 Factor of safety map for Case 1a with uniform soil thickness at 1 hour after the Landslide A failure

The FS maps at 4 hours before and 1 hour after the Landslide A failure have been produced for Case 1b that considered the areas not classified as surficial deposits to be bare rock (Fig. 10(a)). The variation of FS with time for the landslide-producing slope is also compared with the Standard Case that assumes a 0.1m weathered soil layer over these areas (Fig. 10(b)). High-hazard areas (FS <1.2) are already present at 4 hours before the recorded failure for Case 1b, contrasting with the Standard Case (Fig. 5), where slopes were relatively stable at this point. The reason for this quicker reduction in FS is shown in Fig. 11, which presents the lateral surface runoff 4 hours before failure for the case with bare rock (Case 1b). The surface runoff flows into the neighbouring cells covered by superficial deposits faster over bare rock, reducing the soil strength in these cells more efficiently. By contrast, there is no surface runoff at the start of the rainfall event (hour -4) for the Standard Case because the rainfall intensity was less than the Ks of the soil, 8×10^{-6} m/s. These results show the importance of sufficiently and appropriately representing the thickness of soils across a site, and the marked difference that a

thin soil layer can have over bare and exposed rock in governing the behaviour of the slope system.

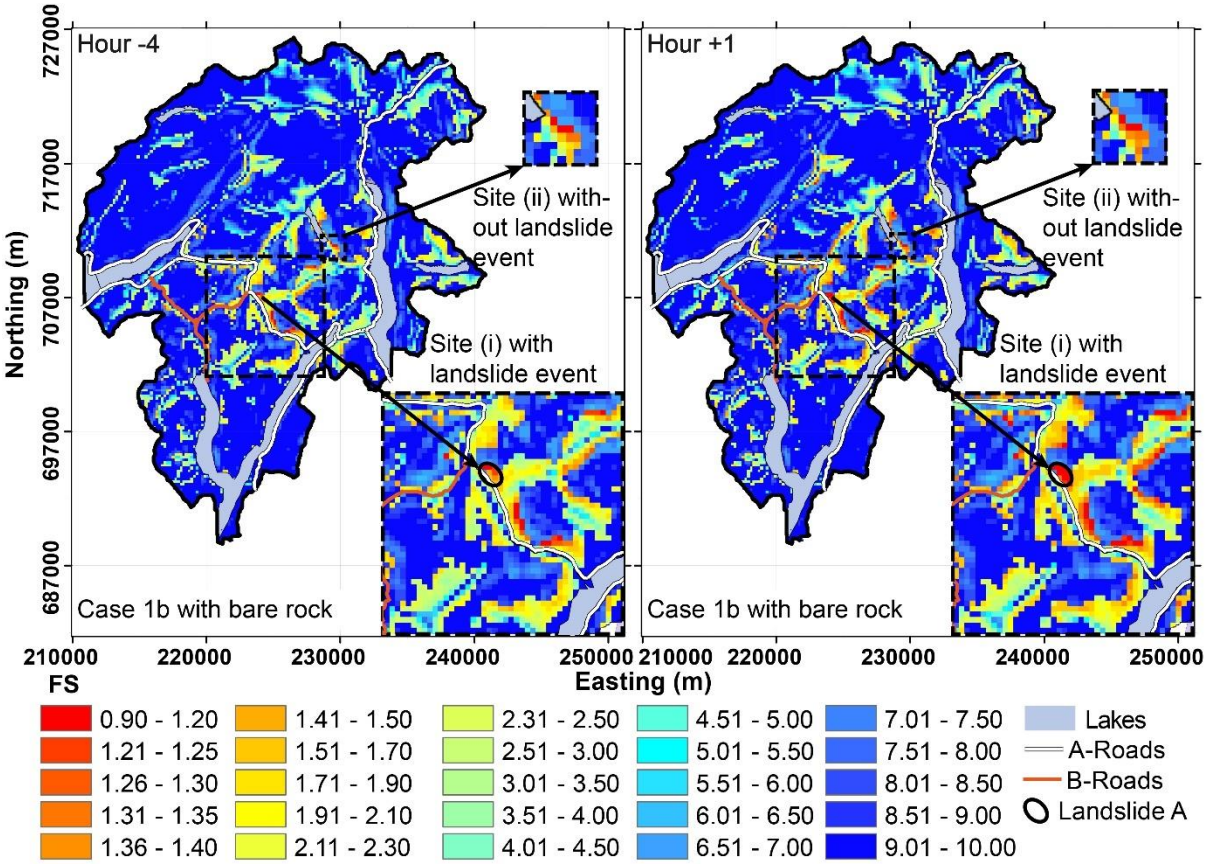

(a) FS map for Case 1b

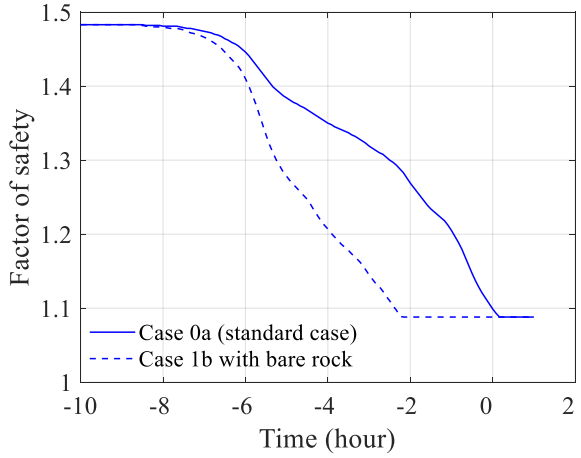

(b) FS variation with time

Fig. 10 Factor of safety for Case 1b with bare rock

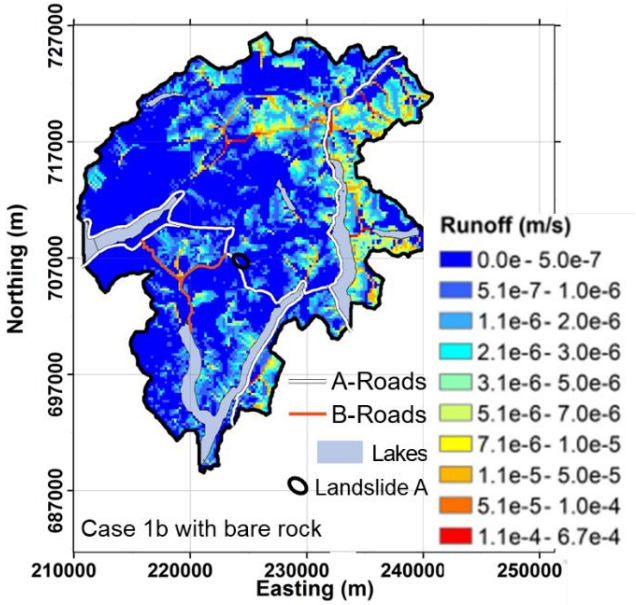

Fig. 11 Surface runoff at 4 hours before the Landslide A failure for Case 1b with bare rock

Effect of soil strength

The FS maps at 4 hours before the Landslide A failure (hour -4) calculated with reduced cohesion (Case 2a) and reduced friction angle (Case 2b) are presented in Fig. 12(a). The variations of FS through the rainfall event for the slope associated with Landslide A are presented in Fig. 12(b). The FS maps show high-hazard areas (FS <1.2) at hour -4 (see the red areas in Fig. 12(a)), indicating that the FS for the two cases is smaller than that of the Standard Case. These results are expected as Cases 2a and 2b have smaller shear strength parameters, resulting in a lower initial FS for the Landslide A slope as shown in Fig. 12(b). Moreover, the differences in FS between Case 2a and the Standard Case remain constant whereas there is a reduced difference between Case 2b and the Standard Case with time (Fig. 12(b)). This can be explained by the expression of the factor of safety for the infinite slopes, given by

$$\mathrm{FS}=\begin{cases}\dfrac{\tan\phi}{\tan\delta}+\dfrac{c\text{-}\varphi(Z,\,t)\gamma_w\tan\phi}{\gamma_s Z\sin\delta\cos\delta} & \text{for saturated soils}\\ \dfrac{\tan\phi}{\tan\delta}+\dfrac{c\text{-}\chi\varphi(Z,\,t)\gamma_w\tan\phi}{\gamma_s Z\sin\delta\cos\delta} & \text{for unsaturated soils}\end{cases} \tag{2}$$

where ϕ is the frictional angle; δ is the slope angle; c is the soil cohesion; Z is the depth of slope; $\varphi(Z, t)$ is the pore water pressure head at depth Z and time t; γ_w and γ_s are the unit weight of the water and soil, respectively; $\chi = (\theta - \theta_r)/(\theta_s - \theta_r)$ is an effective stress parameter to

consider the contribution of suction stress to effective stress. As shown from Eq. 2, the contribution of cohesion to the FS (i.e., $c/\gamma_s Z\sin\delta\cos\delta$) remains constant with time, but the contribution from the friction angle to the FS (i.e., $\tan\phi(\frac{1}{\tan\delta}-\frac{\varphi(Z,t)\gamma_w}{\gamma_s Z\sin\delta\cos\delta})$) reduces with time as the pore water pressure becomes larger as time elapses. As a result, the difference of FS for two slopes with frictional angles of ϕ_1 and ϕ_2 (assume $\phi_1 > \phi_2$), $(\tan\phi_1 - \tan\phi_2)(\frac{1}{\tan\delta}-\frac{\varphi(Z,t)\gamma_w}{\gamma_s Z\sin\delta\cos\delta})$ also reduces with time.

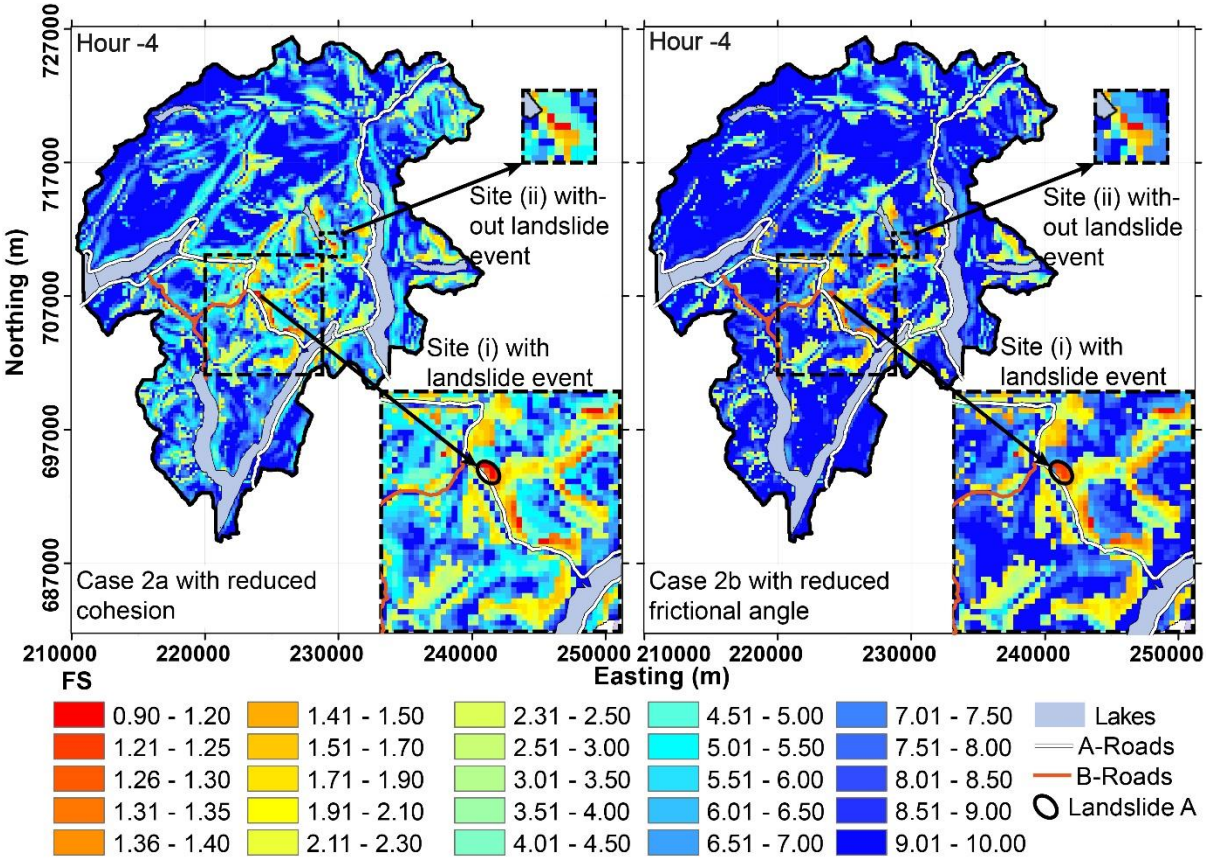

(a) FS maps for cases 2a and 2b at hour -4

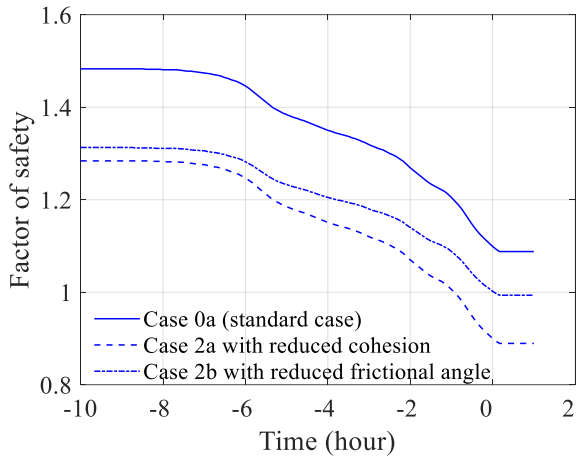

(b) FS variation with time

Fig. 12 Factor of safety for cases 2a and 2b with reduced shear strength

Effect of hydraulic parameters

The effect of four hydraulic parameters, Ks, α, D_0 and initial water table depth on the regional-scale FS map has been investigated. Fig. 13(a-b) shows the FS map with a reduced Ks (Case 3a), with increased α (Case 3b), with increased D_0 (Case 3c) and with a shallower initial water table (Case 3d). By comparing Fig. 13(a) with Fig. 5, it is evident that the FS for reduced Ks and increased α are generally higher than for the Standard Case, evidenced by the limited number of high-hazard cells, namely cells with an FS < 1.2 just after the failure occurrence. The FS variation through the duration of the rainfall event at the Landslide A slope is also presented (Fig. 13(c)). The FS difference between the Standard Case and Case 3a with reduced Ks at the point of slope failure was 0.15 but a large difference (0.4) was noted between the FS in the Standard Case and Case 3b with increased α. A smaller value of Ks and a larger value of α lead to a slower infiltration rate, and, in turn, slow the reduction in the shear strength of slope materials. Fig. 13(d) shows the hydraulic conductivity curves become steeper as α increases, meaning that the unsaturated zone is less permeable for a large α and the infiltration rate is reduced.

The FS for increased D_0 (Case 3c) and shallower initial water tables (case 3d) is generally lower than that for the Standard Case. High-hazard cells (FS < 1.2) are observed in the FS maps

at 4 hours before the Landslide A failure (hour -4) for cases 3c and 3d (Fig. 13(b)). The FS for the increased D_0 case drops more rapidly than the Standard Case while consideration of a shallower initial water table produces a smaller initial value of FS (Fig. 13(c)). This is because a larger value of D_0 results in more rapid spreading of water through the soil medium while a shallower initial water table produces a higher pore water pressure and a lower soil shear strength. These results demonstrate the importance of identifying the actual value of the four hydraulic parameters, Ks, α, D_0 and initial water table depth to attain the most accurate starting values of FS.

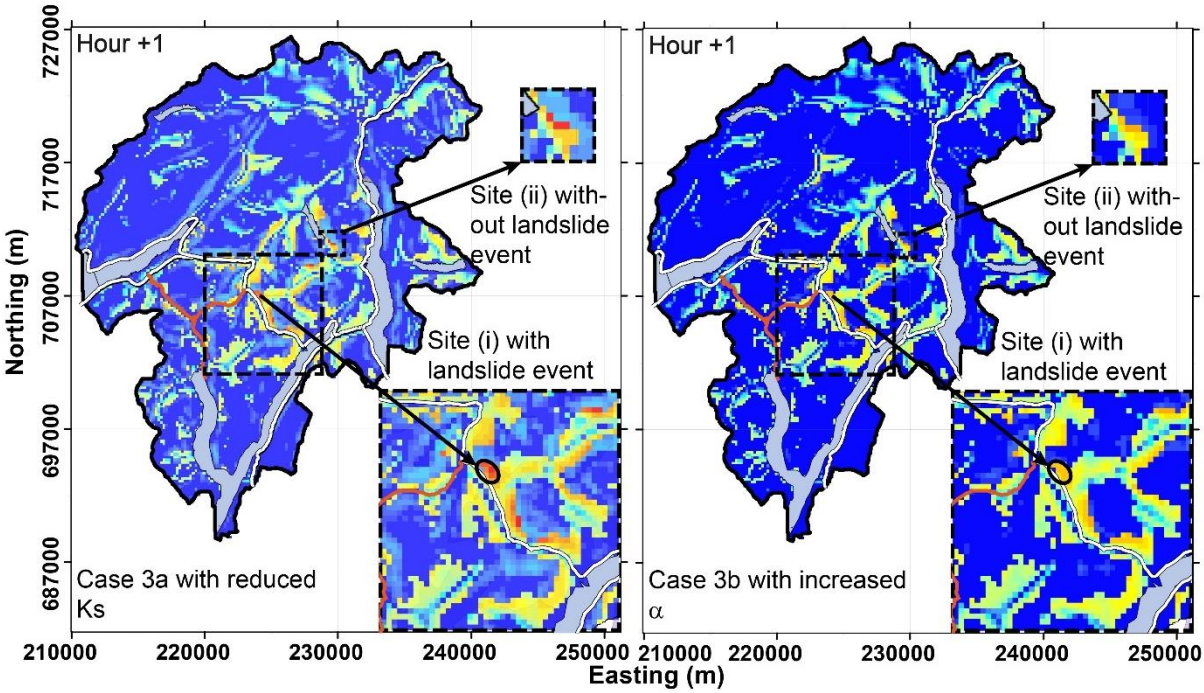

(a) FS maps for cases 3a and 3b at hour +1

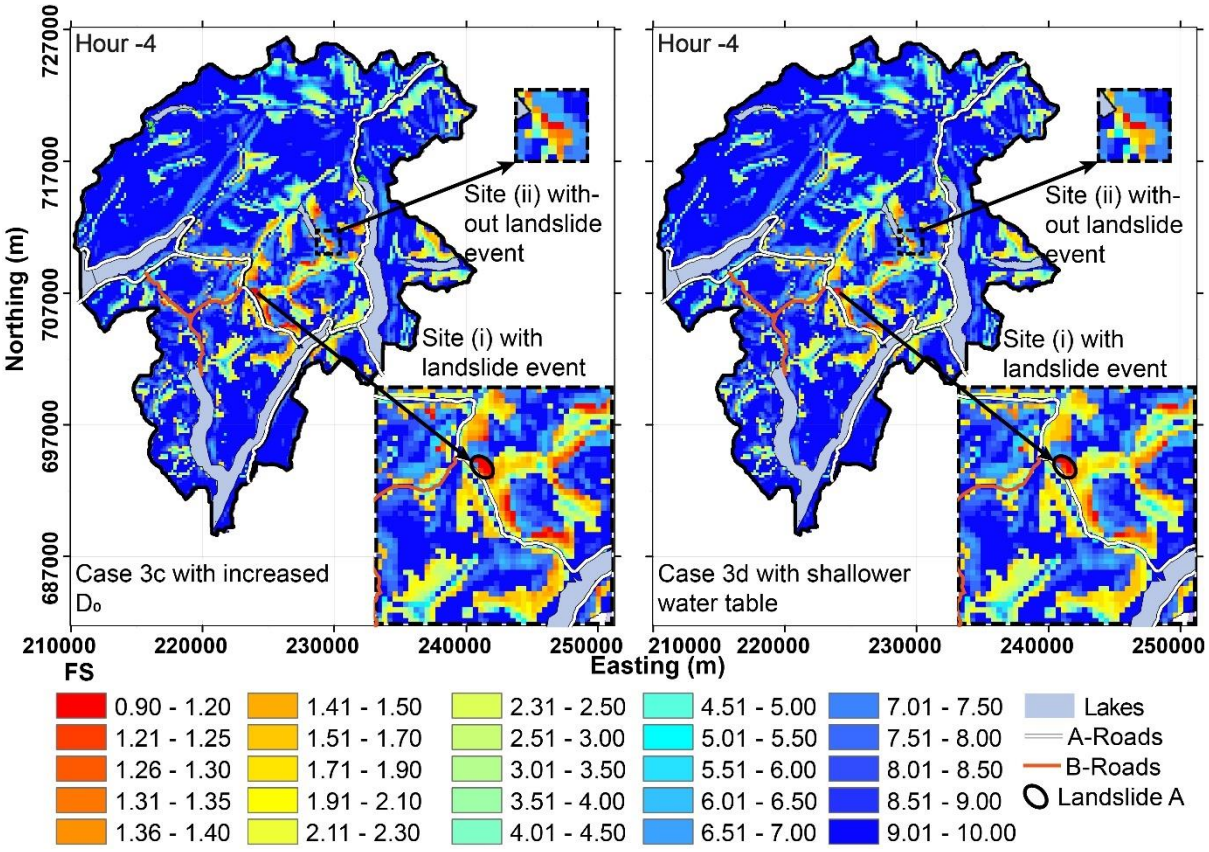

(b) FS maps for cases 3c and 3d at hour -4

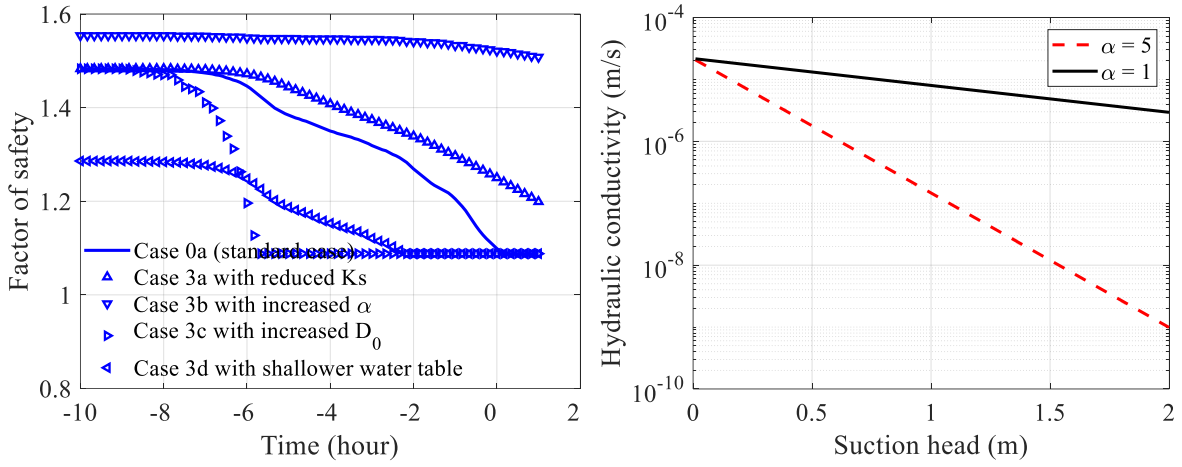

(c) FS variation with time (d) Hydraulic conductivity

Fig. 13 Factor of safety for case 3a-3d with different hydraulic parameters

Effect of antecedent rainfall

The effect of antecedent rainfall on the regional-scale FS map (Fig. 14(a)) and change in the FS through time at the Landslide A slope failure location (Fig. 14(b)) has been investigated. There are already some high-hazard areas (FS <1.2) before the main rainfall event (hour -4) because the FS has been reduced relative to the Standard Case by the antecedent rain. The

reduction in FS is initially dramatic with a high sensitivity to additional rainfall before a more gradual decline, reaching its lowest value 3 hours before the Standard Case.

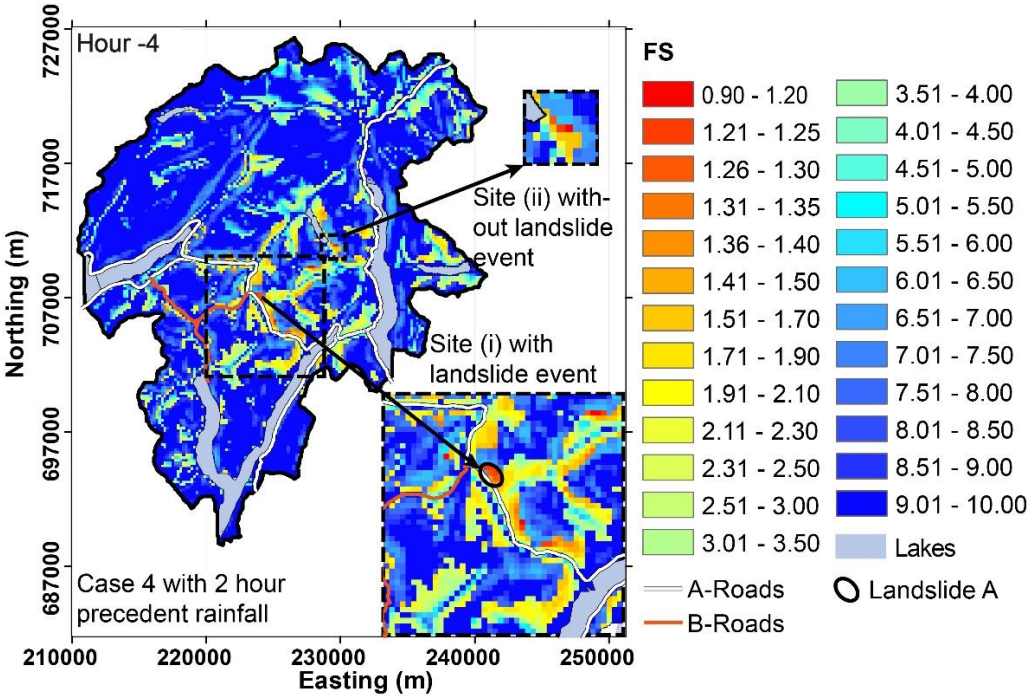

(a) FS map at hour -4

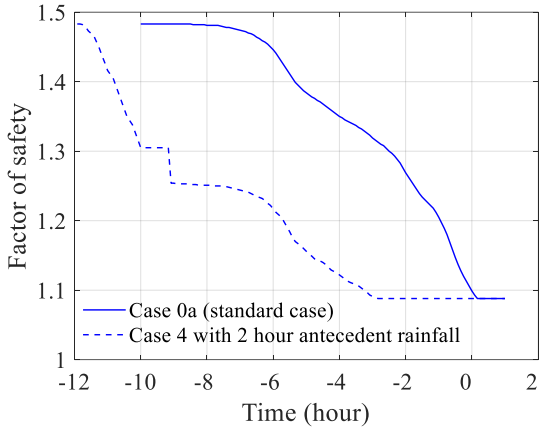

(b) FS variation with time

Fig. 14 Factor of safety for Case 4 with antecedent rainfall

Parameter significance for shallow landslide early warning applications

Analyses of the nine cases in Table 3 have shown that physical parameters can play a varied role in the stability of slopes at a regional scale. An appreciation of the different influence parameters can have on the FS can guide site investigation efforts to the most critical parameters to better constrain. The ΔFS is defined as the difference between the FS for any case at a certain time and location and the FS produced by the Standard Case, $FS_{standard}$. Fig.

15 plots the variation of ΔFS with time for Landslide A slope (Fig. 15a), the histogram of FS and ΔFS for relatively high-hazard slopes with $FS_{standard}$ < 3 at hour -1 (Fig. 15b, c). This comparative analysis demonstrates that the FS is particularly sensitive to the saturated hydraulic diffusivity parameter, D_0, Gardner's unsaturated conductivity model, α, the initial water table depth, shear strength, and antecedent rainfall. The D_0 and α mainly affect the reduction rate of the FS of a slope during rainfall events whereas the shear strength, initial water table depth, and antecedent rainfall primarily influence the initial value of the FS. Therefore, the former set should be focused upon if the decisions are based on a rate of change in the FS, but the latter four parameters are most important if the decision-making thresholds are based on a set value of FS.

The minimum FS of the slope is determined mainly by the shear strength of saturated soils rather than hydraulic parameters. The hydraulic parameters primarily affect the time it takes to saturate the slope. More detailed, site-specific information on the most influential parameters will produce more accurate dynamic FS maps and hence improve the identification of the high-hazard areas for any particular rain event. Furthermore, the histogram also shows how many slopes would be of concern in the presence of particularly uncertain soil properties. For example, Fig. 15(b) shows that 40 slopes (or 0.25% of the catchment area) may have high hazard (i.e., FS < 1.2) at hour -1 in the most critical case, i.e., case 3c with increased D_0.

A 'real-time' early warning map incorporating both FS and δ_{FS} information can now be generated in response to spatially and temporally complex rainfall events, each generating a unique distribution of water into slope systems. For example, Fig. 16 presents the landslide risk map 1 hour before the Landslide A failure, combining the dynamic FS maps of the Standard Case. The highest risk level (level 1) is associated with both a relatively low value of FS (< 1.2) and a relatively low value of δ_{FS} (< -0.2) at hour -1, while for the medium risk level (level 2a and 2b), only one of the two indexes has a relatively low value (either FS < 1.2 or δ_{FS} < -

0.2). The relatively low level pertains to a relatively high FS and δ_{FS} (1.2 < FS < 1.4 and δ_{FS} > -0.2). The δ_{FS} index serves as a good complement of the FS as it measures the evolution of the landslide occurrence risk. More importantly, the δ_{FS} index is less sensitive to the input parameters, which is evident in Fig. 15(a, c). Indeed, five cases including the standard case, Case 2a with reduced c, Case 2b with reduced ϕ, Case 3d with a shallower initial water table and Case 4 with 2-hour antecedent rainfall have similar values of δ_{FS} as their ΔFS curves are almost parallel to each other. In this regard, it is a reliable way to use the δ_{FS} to identify the high-hazard areas and could for instance be used to increase the frequency of slope movement monitoring at key sites (Khan et al. 2021).

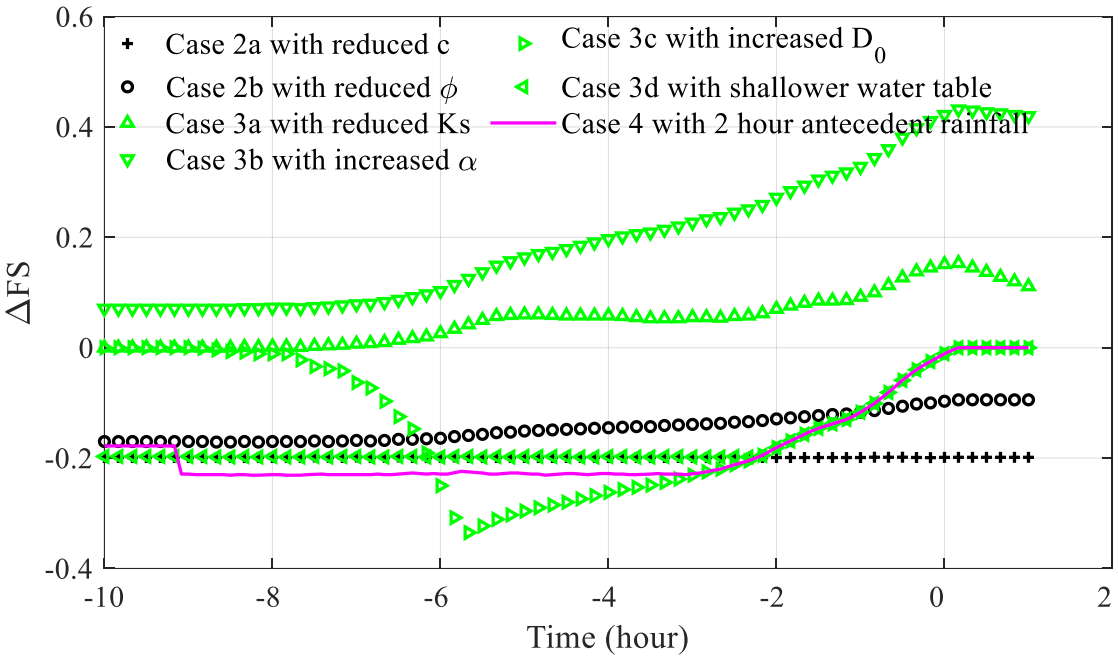

(a) Δ_{FS} for landslide A slope

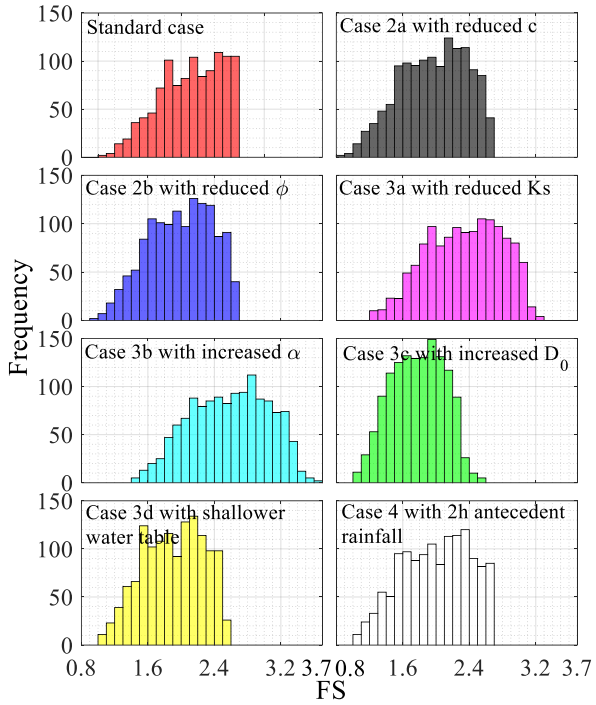

(b) Histogram of FS for slopes with $FS_{standard} < 3$ at hour -1

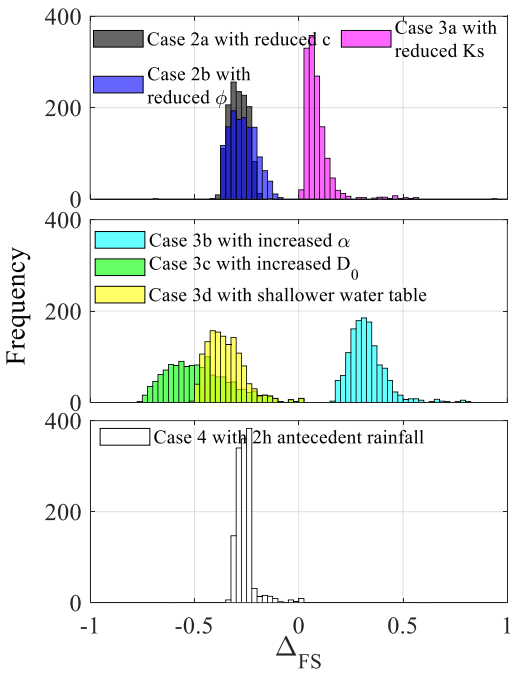

(c) Histogram of Δ_{FS} for slopes with $FS_{standard} < 3$ at hour -1 (figures split for clarity)

Fig. 15 Sensitivity of FS to various parameters

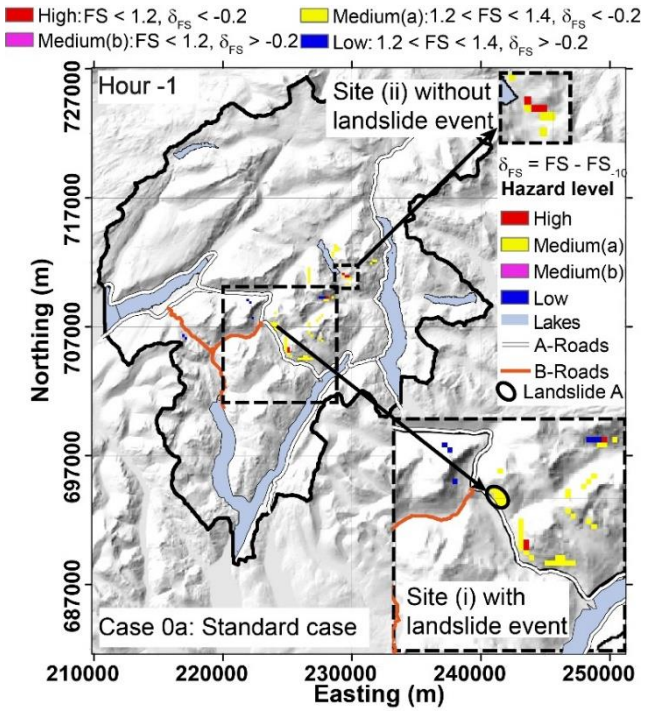

Fig. 16 Early warning of landslide hazard based on dynamic FS maps

Conclusions

The study has developed and applied a procedure for real-time hazard assessment of shallow landslides on a regional scale. A physically based program, TRIGRS, was used to evaluate the

factor of safety (FS) for slopes on a regional scale in response to spatially and temporally specific rainfall radar data. Dynamic FS maps were produced for early warning or decision-making across regional-scale infrastructure operations impacted by extreme events. The proposed procedure has been demonstrated at a well-known landslide hazard area round Glen Croe, western Scotland. To consider the uncertainty of various parameters, the sensitivity of the dynamic FS map to the soil thickness, shear strength, hydraulic parameters, and antecedent rainfall conditions were investigated. The following conclusions are drawn from the analyses.

(1) The high-hazard areas of the watershed identified with the procedure during an actual high-intensity rainfall period correspond well with the sites where actual landslides occurred during that event. The dynamic FS map can issue an early warning for slopes across a wide scale that are approaching a critical threshold or where stability is changing most rapidly in response to rainfall. The current practice that uses a spatially constant site-specific rainfall intensity across wide regions, may induce significant biases (such as an overestimation of 1.6) of the FS of slopes. The new procedure developed can identify the slopes with relatively high hazards, which account for a small percentage (<1%) of the whole watershed. This facilitates a better and more effective planning and targeted deployment of resources to these relatively small but critical areas.

(2) The selection of the soil thickness model significantly affects the sensitivity of the FS map. Using a uniform soil thickness across the region generally overestimates the soil thickness over shallow or exposed rock layers, resulting in an unrealistic overestimation of the high-hazard areas. In contrast, a rock layer treated as bare rock induces extra surface runoff in seepage analyses, leading to an underestimation of the FS if thin layers of soil are present. Hence, it is beneficial to identify the actual thickness of the soil layers at key sites to improve hazard analyses.

(3) Both the strength parameters and hydraulic parameters play a vital role in the evolution of the FS of slopes. The saturated hydraulic diffusivity D_0 and Gardner's unsaturated conductivity model parameter α mainly affect the reduction rate of the FS of a slope during rainfall events whereas the shear strength, initial water table depth, and antecedent rainfall primarily affect the initial value of the FS. The minimum value of FS of slopes is determined by the shear strength parameters. These parameters need to be further explored and identified through site investigations.

(4) Where wide areas are considered because of the extent of the operational interests or the magnitude of the rainfall event, datasets on key parameters are likely to be available at coarse resolution. However, it has been shown that by analysing the change in FS with time (δ_{FS}) rather than absolute thresholds for slopes where failure is a real possibility (FS<1.6), uncertainty in parameters can be negated and effective hazard maps produced. This approach enables mitigation and remediation efforts to be targeted for each unique storm event that impacts extensive areas.

Acknowledgements

We thank NERC (NE/P000010/1, NE/T00567X/1, NE/T005653/1), and Transport Scotland and the Scottish Road Research Board (SRRB) for funding.

Declarations

Competing interests **The authors declare no competing interests.**

References

Akgun A (2012) A comparison of landslide susceptibility maps produced by logistic regression, multi-criteria decision, and likelihood ratio methods: A case study at İzmir, turkey. Landslides 9: 93-106.

Argyroudis S A, Mitoulis S A, Winter M G and Kaynia A M. 2019. Fragility of transport assets exposed to multiple hazards: state-of-the-art review toward infrastructure resilience. Reliability Engineering and System Safety 191: 1-22.

Arnone E, Noto L, Lepore C and Bras R (2011) Physically-based and distributed approach to analyze rainfall-triggered landslides at watershed scale. Geomorphology 133: 121-131.

Ayalew L, Yamagishi H and Ugawa N (2004) Landslide susceptibility mapping using GIS-based weighted linear combination, the case in Tsugawa area of Agano river, Niigata Prefecture, Japan. Landslides 1: 73-81.

Bainbridge R, Lim M, Dunning S, Winter M G, Diaz-Moreno A, Martin J, Torun H, Sparkes B, Khan M W and Jin N (2022) Detection and forecasting of shallow landslides: lessons from a natural laboratory. Geomatics, Natural Hazard and Risk 13(1): 686-704.

Baum RL, Savage WZ and Godt JW (2002) TRIGRS—a Fortran program for transient rainfall infiltration and grid-based regional slope-stability analysis. US geological survey open-file report, 2.0 eds.

Baeza C, Lantada N and Moya J (2010) Validation and evaluation of two multivariate statistical models for predictive shallow landslide susceptibility mapping of the eastern Pyrenees (Spain). Environmental Earth Sciences 61: 507-523.

Borga M, Dalla Fontana G, Da Ros D and Marchi L (1998) Shallow landslide hazard assessment using a physically based model and digital elevation data. Environmental geology 35: 81-88.

BGS (1987). Ben Lomond. Scotland Sheet 38W. Solid. 1:50,000 Geological Map Series. British Geological Survey, Keyworth, Nottingham.

Canli E and Glade T (2016) Dynamic, physical-based landslide susceptibility modelling based on real-time weather data. EGU General Assembly Conference Abstracts, pp EPSC2016-2414

Cascini L, Ciurleo M, Di Nocera S and Gullà G (2015) A new–old approach for shallow landslide analysis and susceptibility zoning in fine-grained weathered soils of southern italy. Geomorphology 241: 371-381.

Chen HX and Zhang LM (2014) A physically-based distributed cell model for predicting regional rainfall-induced shallow slope failures. Engineering geology 176: 79-92.

Chen Y-l, Chen D-h, Li Z-c and Huang J-b (2016) Preliminary studies on the dynamic prediction method of rainfall-triggered landslide. Journal of Mountain Science 13: 1735-1745.

Clarke BG (2018) The engineering properties of glacial tills. Geotechnical Research 5: 262-277.

Dikshit A, Satyam N and Pradhan B (2019) Estimation of rainfall-induced landslides using the TRIGRS model. Earth Systems and Environment 3: 575-584.

Erener A and Düzgün HSB (2010) Improvement of statistical landslide susceptibility mapping by using spatial and global regression methods in the case of More and Romsdal (Norway). Landslides 7: 55-68.

ESRI, Environmental Systems Research Institute (2016) ArcGIS desktop 10.5. Esri Redland, California, U.S.

Felicísimo ÁM, Cuartero A, Remondo J and Quirós E (2013) Mapping landslide susceptibility with logistic regression, multiple adaptive regression splines, classification and regression trees, and maximum entropy methods: A comparative study. Landslides 10: 175-189.

Finlayson A (2020) Glacial conditioning and paraglacial sediment reworking in Glen Croe (the Rest and Be Thankful), western Scotland. Proceedings of the Geologists' Association 131: 138-154.

Gardner W (1958) Some steady-state solutions of the unsaturated moisture flow equation with application to evaporation from a water table. Soil science 85: 228-232.

Gioia E, Speranza G, Ferretti M, Godt JW, Baum RL and Marincioni F (2016) Application of a process-based shallow landslide hazard model over a broad area in central Italy. Landslides 13: 1197-1214.

Gibson A, Culshaw M, Dashwood C and Pennington C (2013) Landslide management in the UK—the problem of managing hazards in a 'low-risk'environment. Landslides 10: 599-610.

Handwerger AL, Jones SY, Huang M-H, Amatya P, Kerner HR and Kirschbaum DB (2020) Rapid landslide identification using synthetic aperture radar amplitude change detection on the google earth engine. Natural Hazards and Earth System Sciences Discussions: 1-24.

Harrison M, Gibson A, Forster A, Entwisle D and Wildman G (2008) GIS-based assessment. In: Winter M, Macgregor F and Shackman L (eds) Scottish road network landslides study: Implementation, Transport Scotland, Edinburgh, UK.

Hsu Y-C, Chang Y-L, Chang C-H, Yang J-C and Tung Y-K (2018) Physical-based rainfall-triggered shallow landslide forecasting. Smart Water 3: 3. doi: 10.1186/s40713-018-0011-8

Hsu Y-C and Liu K-F (2019) Combining TRIGRS and debris-2d models for the simulation of a rainfall infiltration induced shallow landslide and subsequent debris flow. Water 11: 890.

Khan MW, Dunning S, Bainbridge R, Martin J, Diaz-Moreno A, Torun H, Jin N, Woodward J and Lim M (2021) Low-cost automatic slope monitoring using vector tracking analyses on live-streamed time-lapse imagery. Remote Sensing 13: 893.

Kirschbaum D and Stanley T (2018) Satellite-based assessment of rainfall-triggered landslide hazard for situational awareness. Earth's Future 6: 505-523. doi: https://doi.org/10.1002/2017EF000715

Klose M, Damn B and Terhorst B (2015): Landslide cost modelling for transportation infrastructures: a methodological approach. Landslides 12, 321–334,

Ku C-Y, Liu C-Y, Su Y, Xiao J-E and Huang C-C (2017) Transient modeling of regional rainfall-triggered shallow landslides. Environmental Earth Sciences 76: 1-18.

Lawley R and Garcia-Bajo M (2009) The national superficial deposit thickness model. In: Lawley R, Walsby J and Harrison M (eds), 5 eds. British Geological Survey.

Lee EM and Giles DP (2020) Chapter 4 Landslide and slope stability hazard in the UK. Geological Society, London, Engineering Geology Special Publications 29: 81-162. doi: 10.1144/egsp29.4

Liu C-N and Wu C-C (2008) Mapping susceptibility of rainfall-triggered shallow landslides using a probabilistic approach. Environmental Geology 55: 907-915.

Mathew J, Jha V and Rawat G (2009) Landslide susceptibility zonation mapping and its validation in part of Garhwal Lesser Himalaya, India, using binary logistic regression analysis and receiver operating characteristic curve method. Landslides 6: 17-26.

Milne FD (2008) Topographic and material controls on the Scottish debris flow geohazard. Ph.D. thesis, University of Dundee.

Montrasio L, Valentino R and Losi G (2011) Towards a real-time susceptibility assessment of rainfall-induced shallow landslides on a regional scale. Natural hazards and earth system sciences 11: 1927-1947.

Marin RJ (2020) Physically based and distributed rainfall intensity and duration thresholds for shallow landslides. Landslides 17: 2907-2917. doi: 10.1007/s10346-020-01481-9

Marin RJ, García EF and Aristizábal E (2021) Assessing the effectiveness of trigrs for predicting unstable areas in a tropical mountain basin (Colombian Andes). Geotechnical and Geological Engineering 39: 2329-2346.

Prasetya H, Aditama T, Sastrawiguna G, Rizqi A and Zamroni A (2021) Analytical landslides prone area by using sentinel-2 satellite imagery and geological data in google earth engine (a case study of cinomati street, bantul regency, daerah istimewa yogyakarta province, indonesia). IOP Conference Series: Earth and Environmental Science, IOP Publishing, pp 022025.

Remondo J, Bonachea J and Cendrero A (2005) A statistical approach to landslide risk modelling at basin scale: From landslide susceptibility to quantitative risk assessment. Landslides 2: 321-328.

Segoni S, Piciullo L and Gariano SL (2018) A review of the recent literature on rainfall thresholds for landslide occurrence. Landslides 15: 1483-1501. doi: 10.1007/s10346-018-0966-4

Teixeira M, Bateira C, Marques F and Vieira B (2015) Physically based shallow translational landslide susceptibility analysis in Tibo catchment, NW of Portugal. Landslides 12: 455-468.

Winter, M G. 2020. Debris flows. In: Geological hazards in the UK: their occurrence, monitoring and mitigation – Engineering Group Working Party Report (Eds: Giles, D P and Griffiths, J S). Engineering Geology Special Publication 29, 163-185. Geological Society, London.

Winter M G and Wong, J C F (2020) The assessment of quantitative risk to road users from debris flow. Geoenvironmental Disasters 7(4): 1-19.

Winter, M G, Dent, J, Macgregor, F, Dempsey, P, Motion, A and Shackman, L (2010). Debris flow, rainfall and climate change in Scotland. Quarterly Journal of Engineering Geology and Hydrogeology, 43(4), 429-446.

Winter M G, Smith J T, Fotopoulou S, Pitilakis K, Mavrouli O, Corominas J and Argyroudis S (2014) An expert judgement approach to determining the physical vulnerability of roads to debris flow. Bulletin of Engineering Geology and the Environment 73(2): 291-305.

Winter M G, Ognissanto F and Martin L A (2019a) Rainfall thresholds for landslides: deterministic and probabilistic approaches. Published Project Report PPR 991. Transport Research Laboratory, Wokingham.

Winter M G, Peeling D, Palmer D and Peeling J. (2019b) Economic impacts of landslides and floods on a road network. AUC Geographica 54(2): 207-220.

Xie M, Esaki T and Cai M (2004) A time-space based approach for mapping rainfall-induced shallow landslide hazard. Environmental Geology 46: 840-850.

Zieher T, Rutzinger M, Schneider-Muntau B, Perzl F, Leidinger D, Formayer H and Geitner C (2017) Sensitivity analysis and calibration of a dynamic physically based slope stability model. Natural Hazards and Earth System Sciences 17: 971-992.